ARTICLE

Photoionization and Dissociation Study of 2-Methyl-2-propen-1-ol: Experimental and Theoretical Insights

Ye-peng Yu, Zhao-hui Li, Xuan Lin, Jun Chen, Hang Zhang, Yan-bo Li, Huang-huang Wang, Rui-rui Sun, Qing-hui Meng, Xiao-bin Shan, Fu-yi Liu*, Liu-si Sheng

National Synchrotron Radiation Laboratory, University of Science and Technology of China, Hefei 230029, China

(Dated: Received on May 3, 2018; Accepted on June 3, 2018)

The photoionization and dissociation of 2-methyl-2-propen-1-ol (MPO) have been investigated by using molecular beam experimental apparatus with tunable vacuum ultraviolet synchrotron radiation in the photon energy region of 8.0−15.5 eV. The photoionization efficiency (PIE) curves for molecule ion and fragment ions: $C_4H_8O^+$, $C_4H_7O^+$, $C_3H_5O^+$, $C_4H_7^+$, $C_4H_6^+$, $C_4H_5^+$, $C_2H_4O^+$, $C_2H_3O^+$, $C_3H_6^+$, $C_3H_5^+$, $C_3H_3^+$, CH_3O^+, CHO^+ have been measured, and the ionization energy (IE) and the appearance energies (AEs) of the fragment ions have been obtained. The stable species and the first order saddle points have been calculated on the CCSD(T)/cc-pvTZ//B3LYP/6-31+G(d,p) level. With combination of theoretical and experimental results, the dissociative photoionization pathways of 2-methyl-2-propen-1-ol are proposed. Hydrogen migrations within the molecule are the dominant processes in most of the fragmentation pathways of MPO.

Key words: 2-Methyl-2-propen-1-ol, Synchrotron radiation, Photoionization, Vacuum ultraviolet, Mass spectrometry

I. INTRODUCTION

The volatile organic compound (VOC) inventory prepared by the U.S. Environmental Protection Agency (2005), shows that more than 1.7 million tons of oxygen-containing volatile organic compounds (OVOCs) are discharged per year from anthropogenic sources in the USA [1–3]. Incomplete combustion of fossil fuels is the major source of the emissions: off-highway sources (15%), vehicular emissions (30%), and emissions from solvent use (30%). OVOCs are active organic compounds that are emitted into the atmosphere through a number of natural and anthropogenic sources, among which marine air is an important source [4]. Unsaturated alcohols are an important class of OVOCs. Previous investigations [5–8] show the main removal processes of gas-phase unsaturated alcohols (including MPO) in the atmosphere are through the reactions with the atmospheric oxidants, such as Cl atom, OH, O_3, and NO_3 radicals. Besides, MPO plays an important role in industry, where it is applied as a monomer for the synthesis of polymers and as a starting material in the synthesis of pharmaceuticals, pesticides and other allyl compounds [9, 10].

Previous work has been principally concentrated on the removing mechanism and reaction rate coefficients of MPO with OH radical or Cl atom in the atmosphere [8, 11]. Despite the extensive studies performed, some physicochemical properties of MPO, for instance, its IE of parent molecule and AEs of photo-dissociative fragment ions, are not definitely ascertained yet. To the extent of our knowledge, there have been only two studies [12, 13] on the ionization of MPO wherein the IE of MPO has been determined to be 9.24 and 9.28 eV, respectively, and only one fragment ion has been identified as $C_2H_5^+$. The thorough dissociative photoionization of MPO, in experiment or in theory, is still less comprehended. For this purpose, we perform a study on dissociative photoionization process with vacuum ultraviolet (VUV) source ranging over 8.0−15.5 eV. From photoionization efficiency curves, the IE of MPO and AEs of related cations from fragmentation are obtained. With aid of theoretical calculations, our group proposes the fragmental mechanism for the photoionization process of MPO.

II. EXPERIMENTAL METHOD

The experimental apparatus has been depicted comprehensively elsewhere [14–16], and only a brief description is given here. The dissociative photoionization of MPO has been obtained by using reflectron time-of-flight (TOF) spectrometer with supersonic expansion molecular beam. As the ionization source of mass spec-

*Author to whom correspondence should be addressed. E-mail: fyliu@ustc.edu.cn

trometer, the synchrotron radiation from the 800 MeV electron storage ring of NSRL is designed to be in the 7.5−124 eV photon energy range, monochromized with a grazing incidence spherical grating monochromator, and then filtered through a differentially pumped noble gas filter to remove the high-energy harmonics produced by undulator. Argon (6 Torr) is used as the filter gas to restrain higher order of harmonics.

2-Methyl-2-propen-1-ol (Aladdin Corp.) with purity of 99% is used directly without further treatment. Ar (99.995%) is used as carried gas (1 atm) to carry the sample into a continuous beam nozzle (70 μm in diameter). In order to keep vacuum difference and achieve the formation of ultrasonic jet, the mixed gas (sample and Ar) must go through two 1-mm-diameter skimmers and then reach ionization chamber. For detection, the ions formed by the ionization of synchrotron radiation are then extracted by the repulsive electric field into reflectron-TOF mass spectrometer. All mass spectra of fragment ions can be collected by a multiscaler P7888 (FAST ComTek, Germany). PIE curves are deducted from the mass spectra and then normalized with the photocurrent. The turning point of PIE curve is determined as AEs which has been used widely [17, 18].

III. THEORETICAL METHOD

In this theoretical inquiry, all the geometries of related species are optimized for the possible minima and saddle points by the hybrid density functional theory, B3LYP method with 6-31+G(d,p) as basis set, and the vibrational frequencies are also calculated at this level for zero-point correction. In pursuance of exact energies, calculations at the CCSD(T) [19] level employing the correlation consistent triple ζ basis set cc-pVTZ [20], which has been tested to achieve good agreement between computational and experimental results [21–24], were used to calculate the single-point energy of the sample. All theoretical calculations are carried out at the Supercomputing Center of USTC, Hefei, China, using the Gaussian 09 [25] suite of program.

IV. RESULTS AND DISCUSSION

A. Time-of-flight mass spectra

The tunable nature of synchrotron VUV photoionization allows a soft ionization process near threshold energy, which can prevent the interference of fragment ions. The mass spectra of MPO under energies of 9.5, 12.5, and 15.5 eV, respectively, are demonstrated in FIG. 1. At low energy of 9.5 eV, TOF mass spectrum shows only the parent ion (m/z=72), formed by losing one electron of the olefinic bond of MPO. With increasing the energy to 12.5 eV, more fragment ions: $C_4H_7O^+$ (m/z=71), $C_3H_5O^+$ (m/z=57), $C_4H_6{}^+$ (m/z=54), $C_2H_4O^+$ (m/z=53) and $C_2H_3O^+$ (m/z=43) are emerged. At the high energy of 15.5 eV, other smaller fragment ions of 55 ($C_4H_7{}^+$), 44 ($C_2H_6{}^+$), 41 ($C_3H_5{}^+$), 39 ($C_3H_3{}^+$), 31 (CH_3O^+), and 29 (CHO^+) have been identified. The distribution of the fragments is basically similar to statistics that NIST provided [26]. All observed fragments are believed to be born from parent ion $C_4H_8O^+$ since no signal at mass greater than that of $C_4H_8O^+$ (m/z=72) could be detected. The peak of $C_3H_5O^+$ (m/z=57) has the strongest intensity in the energy ranges studied here, which indicates that $C_3H_5O^+$ is the dominated dissociation pathway of MPO by removing a methyl group.

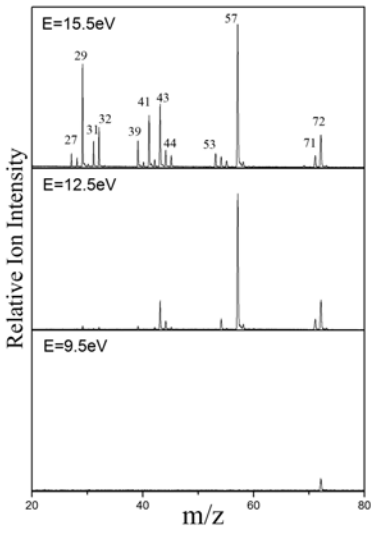

FIG. 1 Photoionization mass spectra of MPO at 9.5, 12.5, and 15.5 eV.

The PIE curves for mother ion $C_4H_8O^+$ as well as fragment ions $C_4H_7O^+$, $C_3H_5O^+$, $C_4H_7{}^+$, $C_4H_6{}^+$, $C_2H_4O^+$, $C_2H_3O^+$, and $C_3H_6{}^+$, are obtained and shown in FIG. 2. The AE values of these fragment ions are determined for the first time by this method. The experimental IE of mother molecule, (9.20±0.03) eV, is in good agreement with the experimental values of 9.28 eV [12] by electron ionization and 9.24 eV by photoionization method [13]. The calculated IE value of parent molecule, 8.94 eV, however, is slightly smaller than the experimental result. The experimental AEs of fragments ($C_4H_7O^+$, $C_3H_5O^+$, $C_4H_7{}^+$, $C_4H_6{}^+$, $C_4H_5{}^+$, $C_2H_5O^+$, $C_2H_4O^+$, $C_2H_3O^+$, $C_3H_6{}^+$, $C_3H_5{}^+$, $C_3H_3{}^+$) are presented in Table I, as well as the calculated IE and AEs of the fragment ions.

B. Dissociation mechanisms

As the increment of photon energy, the fate of different dissociation mechanisms will fall on the parent ions. The geometries of the neutral MPO (P0) and parent ion (P) in the ground states are shown in FIG. 3. Generally, two types of mechanisms for dissociation come in

DOI:10.1063/1674-0068/cjcp1805089

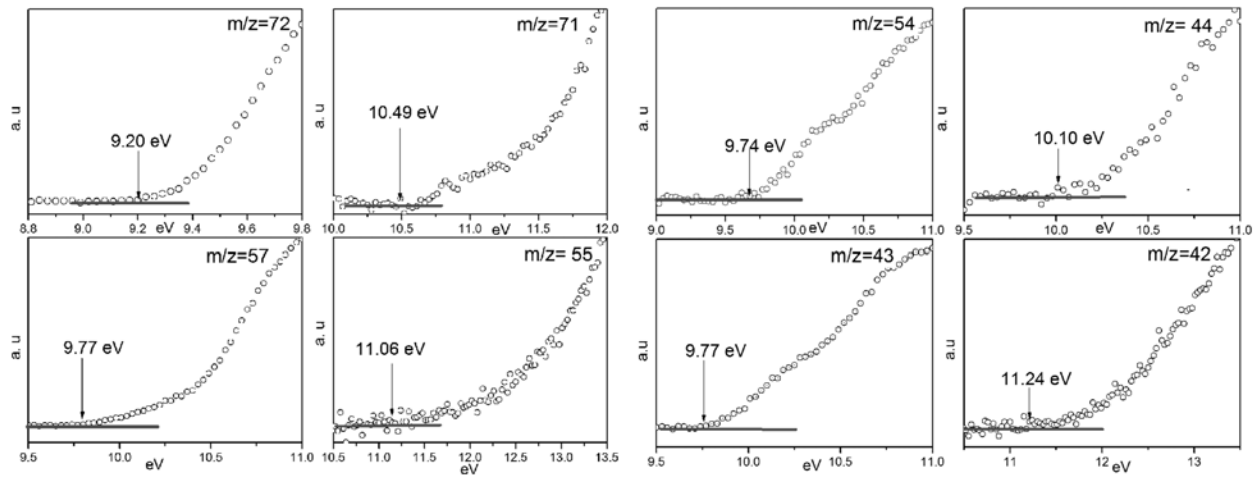

FIG. 2 The normalized PIE curves for fragment ions from dissociative photoionization of MPO.

TABLE I Ionization energy and appearance energies for main fragment ions from dissociative photoionization of MPO, as well as calculation value.

m/z	Ions	IE or AEs / eV			Possible dissociation pathways (this work)
		Experiment	Calculation	Reference	
72	$C_4H_8O^+$	9.20±0.03	8.94	9.28 [12], 9.24 [13]	
71	$C_4H_7O^+$	10.49±0.09	10.09		$C_4H_8O^+ \rightarrow C_4H_7O^+ + H$
57	$C_3H_5O^+$	9.77±0.03	9.87		$C_4H_8O^+ \rightarrow C_3H_5O^+ + CH_3$
55	$C_4H_7^+$	11.06±0.03	11.03		$C_4H_8O^+ \rightarrow C_4H_7^+ + OH$
54	$C_4H_6^+$	9.74±0.03	9.61		$C_4H_8O^+ \rightarrow C_4H_6^+ + H_2O$
53	$C_4H_5^+$	12.35±0.03	12.39		$C_4H_8O^+ \rightarrow C_4H_5^+ + H + H_2O$
44	$C_2H_4O^+$	10.10±0.03	10.19		$C_4H_8O^+ \rightarrow C_2H_4O^+ + C_2H_4$
43	$C_2H_3O^+$	9.77±0.12	10.38	9.69 [13]	$C_4H_8O^+ \rightarrow C_2H_3O^+ + C_2H_5$
42	$C_3H_6^+$	11.24±0.03	11.09		$C_4H_8O^+ \rightarrow C_3H_6^+ + CH_2O$
41	$C_3H_5^+$	12.53±0.03	12.35		$C_4H_8O^+ \rightarrow C_3H_5^+ + CH_2O + H$
39	$C_3H_3^+$	11.75±0.03	11.61		$C_4H_8O^+ \rightarrow C_3H_3^+ + H_2O + CH_3$
31	CH_3O^+	12.23±0.06	12.42		$C_4H_8O^+ \rightarrow CH_3O^+ + CH_3 + C_2H_2$
29	CHO^+	12.20±0.03	12.14		$C_4H_8O^+ \rightarrow CHO^+ + C_2H_4 + CH_3$

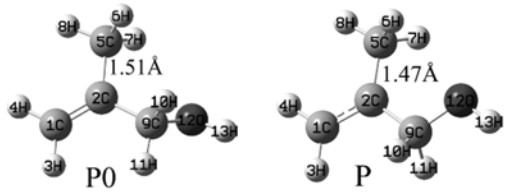

FIG. 3 The geometries of the neutral MPO (P0) and parent ion (P) in the ground states.

our perspective: direct simple bond fission and indirect bond cleavage via transition states and intermediates. The dissociation mechanisms, including both direct and indirect cleavages, will be discussed in detail. The geometries of the related species, products, transition states (TSs), and intermediates (INTs) before and after, involved in the discussion below are shown in FIG. 4 and FIG. 5.

1. The formation pathways of $C_4H_7O^+$ (m/z=71) and $C_4H_7^+$ (m/z=55)

H atom elimination is firstly taken into consideration to form $C_4H_7O^+$ from parent ion $C_4H_8O^+$. The relative energies of $C_4H_7O^+$ calculated at the B3LYP/6-31+G(d,p) level are 10.09 eV (H removing from C5), 11.49 eV (H removing from C9) and 12.54 eV (H removing from O12), respectively. The experimental AE of (10.49±0.09) eV is close to the calculated AE of 10.09 eV (H elimination from C5). Comparing the experimental and calculated results, the pathway of $C_4H_7O^+$ could be hydrogen elimination from C5 in molecule ion.

The fragment $C_4H_7^+$ (m/z=55) can be formed by direct cleavage of C9−O12 bond to lose a OH group.

DOI:10.1063/1674-0068/cjcp1805089

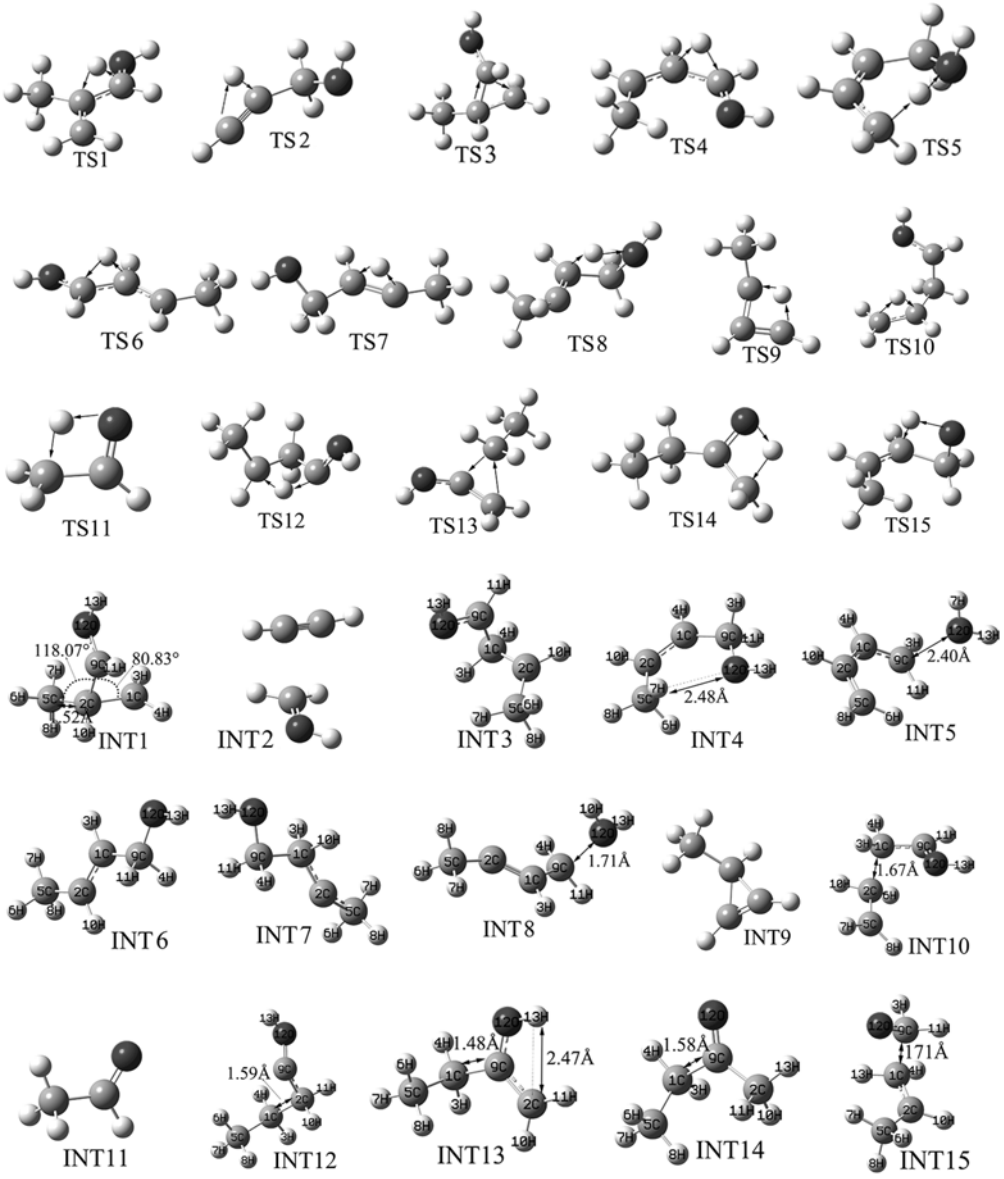

FIG. 4 Geometries of transition states and intermediates obtained under B3LYP method with 6-31+G(d,p) as basis set.

The calculated AE of 11.03 eV using the hybrid density functional theory at B3LYP/6-31+G(d,p) level is in excellent agreement with the experimental value (11.06±0.03) eV, which indicates that the formation pathway of $C_4H_7^+$ is direct fission without barrier.

2. The formation pathways of $C_3H_5O^+$ (m/z=57) and CH_3O^+ (m/z=31)

For the formation of $C_3H_5O^+$ (m/z=57), direct cleavage of C2−C5 bond is at beginning taken into account by losing CH_3 group. The calculated AE for this cation ($CH_2CCH_2OH^+$) is 11.77 eV, which does not agree with experimental value (11.06±0.03) eV. The proposed pathway for the formation of $C_3H_5O^+$ is shown in FIG. 6 via transition state TS1 where H transfers from C9 to C2 with a barrier of 0.94 eV. The calculated AE of $C_3H_5O^+$ is 9.88 eV, which is in reasonable accordance with the experimental result of (9.74±0.03) eV. The most possible configuration of $C_3H_5O^+$ is $CH_2CHCHOH^+$. What is more, this reaction pathway for $C_3H_5O^+$ ion is the dominant dissociative photoionization pathway of MPO.

CH_2OH^+ is initially assumed to come from direct cleavage bond C2−C9 of parent ion by losing neutral CH_2CCH_3. However, the calculation AE value (11.30 eV) is intensively smaller than the value of (12.2±0.03) eV in this work. First, the direct fission of the bond C2−C5 of parent ion forms $CH_2CCH_2OH^+$+CH_3 by crossing an energy barrier of

DOI:10.1063/1674-0068/cjcp1805089

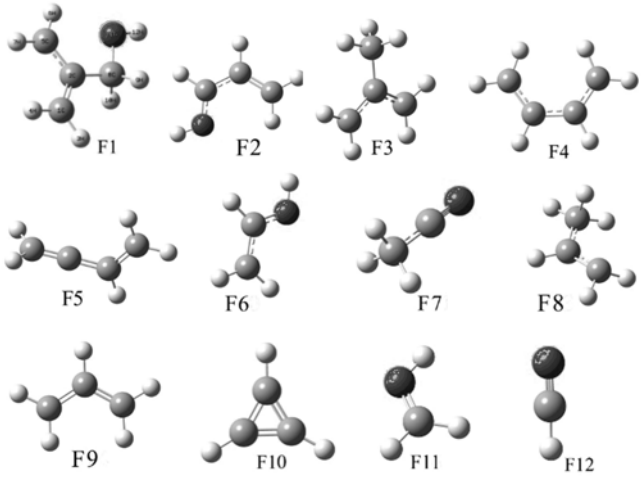

FIG. 5 Geometries of related products optimized with B3LYP/6-31+G(d,p).

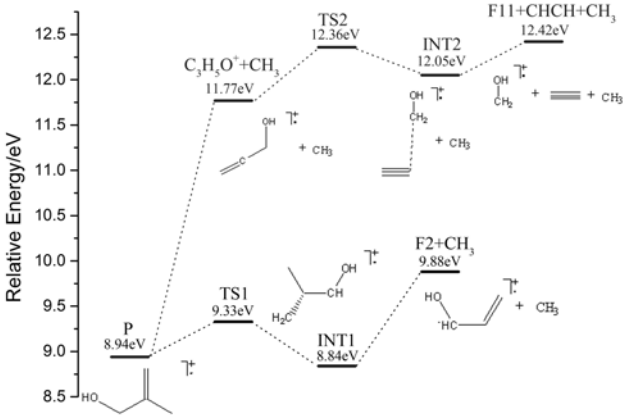

FIG. 6 Formation pathways of $C_3H_5O^+$ and CH_3O^+.

2.83 eV. Second, an H atom on the C1 transfers to C2 passing through a transition state (TS2) to form INT2. Then, the INT15 (CHCHCHOH) loses acetylene to produce CH_2OH^+. Formation pathway of CH_2OH^+ is shown in FIG. 6 and the calculated AE of 12.42 eV is consistent with the experimental value (12.23±0.03) eV.

3. The formation pathways of $C_4H_6^+$ (m/z=54), $C_4H_5^+$ (m/z=53), and $C_3H_3^+$ (m/z=39)

For the formation of the fragment $C_4H_6^+$ (m/z=54), the suggested pathway is described in FIG. 7. First, the CHOH group of INT1 transfers to the C1 across TS3 to form INT3. Second, by overcoming an energy barrier of 0.74 eV, H3 transfers to the C9 by passing through a transition state (TS4) and forms an intermediate (INT4). Then, the INT4 transfers H7 to O12 to form INT5. Due to that the bond C9=O12 of INT5 is much weaker, the $CH_2CHCHCH_2^+$ can be produced by directly breaking this bond. This calculated AE of

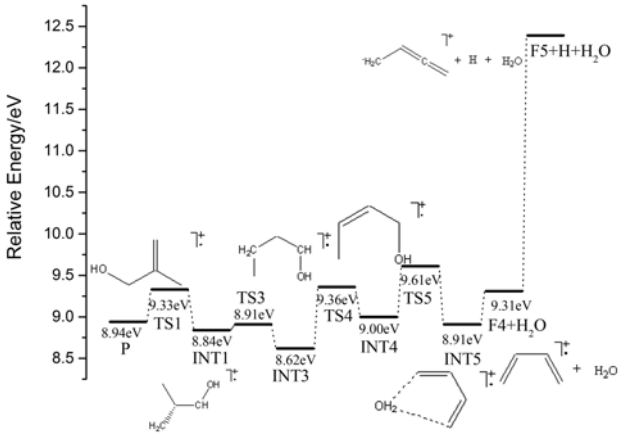

FIG. 7 Formation pathways of $C_4H_6^+$ and $C_4H_5^+$.

$C_4H_6^+$ (m/z=54) is 9.61 eV, which is in good agreement with experimental value (9.74±0.03) eV.

For the production of $C_4H_5^+$ (m/z=53), the parent ion initially loses H_2O to form $CH_2CHCHCH_2^+$ from MPO. The next step, one atomic hydrogen located on the middle carbon of $C_4H_6^+$ (F4) is eliminated to produce the $C_4H_5^+$ (F5). The theoretical AE of $C_4H_5^+$ (12.39 eV) is in excellent agreement with the experimental value (12.35±0.03) eV.

For the formation pathway of $C_3H_3^+$ (m/z=39), H4 of C1 in INT2 firstly transfers to C9 via a transition state (TS6) to form INT6. Secondly, H10 travels to C1 via a transition state of TS7 to form INT7 by overcoming the barrier of 1.4 eV. Thirdly, H10 and H3 have equal chance to contact with O12 to form INT8. As the C9−O12 bond is directly cleaved, the other m/z=54 structure ($CH_3CCHCH_2^+$) can be obtained. This structure of $C_4H_6^+$ ($CH_3CCHCH_2^+$) further loses a methyl group to form $C_3H_3^+$ (m/z=39). Then, one hydrogen shifts from the CH_2 group to the adjacent hydrogenless carbon coupled with a ring closure process through a transition state (TS9) to form INT9 by overcoming an energy barrier of 1.25 eV. The AE of this conformation of $C_3H_3^+$ is 11.61 eV, which is in rough agreement with the experimental value (11.75±0.03) eV (see FIG. 8).

4. The formation pathways of $C_2H_4O^+$ (m/z=44) and CHO^+ (m/z=29)

For the production of $C_2H_4O^+$ (m/z=44), the $C_2H_4O^+$ can proceed by only eliminating CH_2CH_2 group through transferring of one hydrogen atom of methyl of INT3 to adjacent carbon by overcoming an energy barrier of 1.55 eV to generate an intermediate (INT10) where the bond C1−C2 is weak (see FIG. 9). Compared the experimental result of (10.10±0.03) eV with the theoretical calculation value (10.17 eV), the pathway for $C_2H_4O^+$ formation is reasonable.

For the formation of CHO^+, a hydrogen of hydroxyl in $C_2H_4O^+$ (F6) migrates to the methylene through

DOI:10.1063/1674-0068/cjcp1805089

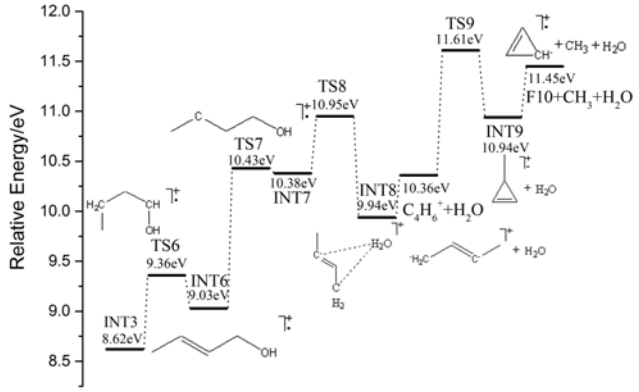

FIG. 8 Formation pathway of $C_3H_3^+$.

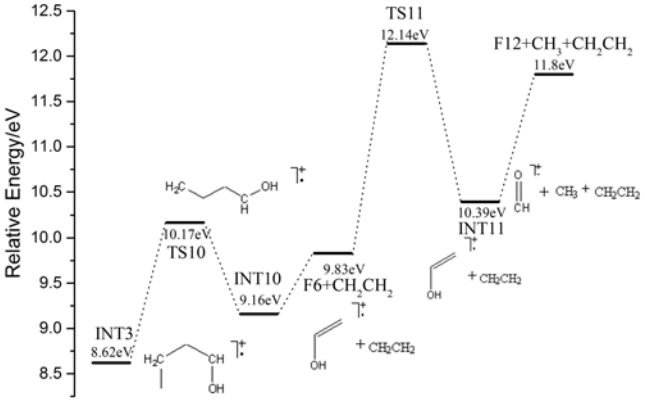

FIG. 9 Formation pathways of $C_2H_4O^+$ and CHO^+.

TS11 with an energy barrier of 2.23 eV to produce CH_3CHCO^+ (INT11), and direct methyl group elimination forms CHO^+. The AE of CHO^+ is calculated to be 12.15 eV, which is consistent with experimental value (12.20±0.03) eV.

5. The formation pathway of $C_2H_3O^+$ (m/z=43)

The roughly linear (excluding hydrogen) fragment $C_2H_3O^+$ (m/z=43) is produced by the pathway: P→INT1→INT3→INT12→INT13→INT14→$C_2H_3O^+$ +C_2H_5 (FIG. 10). One hydrogen on the C9 (INT2) transfers to C2 through TS11 with an energy barrier of 1.51 eV to form INT12, wherein the C1−C2 bond length is elongated from 1.49 Å to 1.59 Å. The process of shifting ethyl in the INT11 to the C9 needs to overcome an energy barrier of 0.94 eV to form TS12 which can then convert into INT13. Subsequently, one hydrogen of the hydroxyl in INT13 transfers to yield 2-butanone cation (INT14) via transition state TS14. $C_2H_3O^+$ is generated by C−C bond cleavage in INT14. The highest barrier along the pathway of formation of acetyl cation is 10.38 eV (relative to neutral parent), which is greater than the experimental AE (9.61 eV)

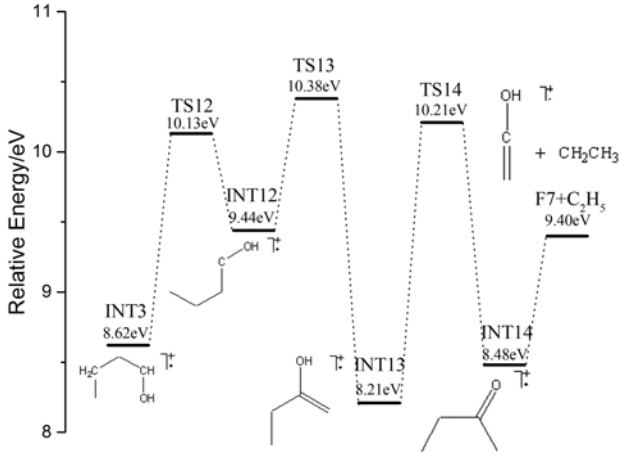

FIG. 10 Formation pathway of $C_2H_3O^+$.

of $C_2H_3O^+$. The reason is not known for the large discrepancy between the theoretical and experimental inquires.

6. The formation pathways of $C_3H_6^+$ (m/z=42) and $C_3H_5^+$ (m/z=41)

The fragment of $CH_3CHCH_2^+$ is suggested via the pathway: P→INT1→INT3→INT4→INT15→ $CH_3CHCH_2^+$+CH_2O (FIG. 11) wherein the first three steps are described above in detail. The migration of hydrogen atom on hydroxyl in INT4 toward the C1 leads to the formation of intermediate INT15 via the transition state TS15 with an energy barrier of 2.09 eV. The bond length of C1−C9 in INT15 is elongated from 1.46 Å to 1.70 Å, making it possible to dissociate fragment $C_3H_6^+$ (m/z=42). The calculated AE of 11.09 eV at the B3LYP/6-31+G(d,p) level, which agrees with the experimental value (11.24±0.03) eV. The fragment ion $C_3H_5^+$ (m/z=41) can be generated with the loss of one hydrogen in methyl from the above fragment ($C_3H_6^+$). The calculated AE of this ion is 12.35 eV, which is closed to experimental value (12.53±0.03) eV.

V. CONCLUSION

The dissociative photoionization of MPO was carried out by photoionization mass spectrometry with synchrotron radiation as ionization source. The ionization energy of MPO and appearance energies for fragment ions were derived from their PIE curves. With help of theoretical calculation on the CCSD(T)/cc-pvTZ//B3LYP/6-31+G(d,p) level, the formation pathways of the dissociation products were explored and twelve possible pathways were proposed—R1: $C_4H_7O^+$+H, R2: $C_4H_7^+$+OH, R3: $C_3H_5O^+$+CH_3,

DOI:10.1063/1674-0068/cjcp1805089

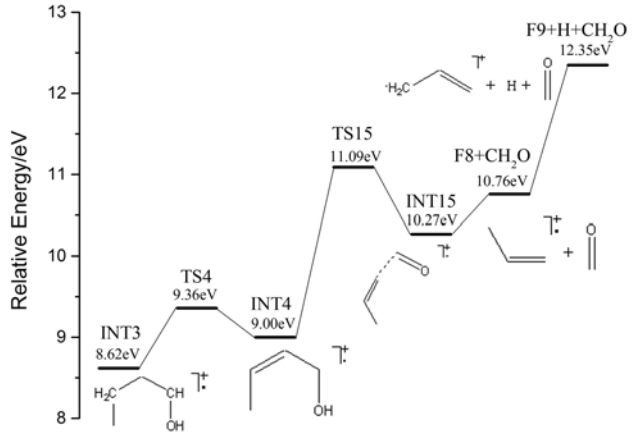

FIG. 11 Formation pathways of $C_3H_6^+$ and $C_3H_5^+$.

R4: CH_2OH^++CHCH+CH_3, R5: $C_4H_6^+$+H_2O, R6: $C_4H_5^+$+H+H_2O, R7: $C_3H_3^+$+CH_3+H_2O, R8: $C_2H_4O^+$+C_2H_4, R9: CHO^++CH_3+C_2H_4, R10: $C_2H_3O^+$+C_2H_5, R11: $C_3H_6^+$+CH_2O, R12: $C_3H_5^+$+H+CH_2O. The dominant processes in most of the dissociative photoionization of MPO are intramolecular hydrogen migrations.

VI. ACKNOWLEDGMENTS

This work was supported by the National Natural Science Foundation of China (No.91544105, No.U1532137, No.275127, No.U1232130, No.U1232209, and No.U11575178) and the Supercomputing Center of USTC is also acknowledged.

[1] A. C. Heiden, K. Kobel, C. Langebartels, G. Schuhthomas, and J. Wildt, J. Atmos. Chem. **45**, 143 (2003).
[2] A. Guenther, C. N. Hewitt, D. Erickson, R. Fall, C. Geron, T. Graedel, P. Harley, L. Klinger, M. Lerdau, W. A. McKay, T. Pierce, B. Scholes, R. Steinbrecher, R. Tallamraju, J. Taylor, and P. Zimmerman, J. Geophys. Res. **100**, 8873 (1995).
[3] P. D. Goldan, W. C. Kuster, and F. C. Fehsenfeld, Geophys. Res. Lett. **20**, 1039 (1993).
[4] C. Schlundt, S. Tegtmeier, S. T. Lennartz, A. Bracher, W. Cheah, K. Krüger, B. Quack, and C. A. Marandino, Atmos. Chem. Phys. **17**, 10837 (2017).
[5] D. Grosjean, E. Grosjean, and E. L. Williams, Int. J. Chem. Kinet. **25**, 783 (1993).
[6] M. Hallquist, S. Langer, E. Ljungström, and I. Wängberg, Int. J. Chem. Kinet. **28**, 467 (1996).
[7] S. A. Peirone, P. M. Cometto, and S. I. Lane, Chemphyschem. **15**, 3848 (2014).
[8] T. D. S. Barbosa, J. D. Nieto, P. M. Cometto, S. I. Lane, G. F. Bauerfeldt, and G. Arbilla, RSC Adv. **4**, 20830 (2014).
[9] V. S. Satam, S. R. Pedada, P. Kamaraj, N. Antao, A. Singh, R. M. Hindupur, H. N. Pati, A. M. Thompson, D. Launay, and D. Martin, Org. Process Res. Dev. **21**, 52 (2017).
[10] C. Tabélé, C. Curti, Y. Kabri, N. Primas, and P. Vanelle, Molecules **20**, 22890 (2015).
[11] A. Rodríguez, D. Rodríguez, A. Soto, I. Bravo, Y. Diaz-de-Mera, A. Notario, and A. Aranda, Atmos. Environ. **50**, 214 (2012).
[12] J. L. Holmes, F. P. Lossing, and P. C. Burgers, Int. J. Mass Spectrom. Ion Processes. **47**, 133 (1983).
[13] J. C. Traeger and D. J. McAdoo, Int. J. Mass Spectrom. Ion Processes. **68**, 35 (1986).
[14] W. Z. Fang, L. Gong, Q. Zhang, X. B. Shan, F. Y. Liu, Z. Y. Wang, and L. S. Sheng, J. Chem. Phys. **134**, 174306 (2011).
[15] M. Wang, J. Chen, W. F. Fei, Z. H. Li, Y. P. Yu, X. Lin, X. B. Shan, F. Y. Liu, and L. S. Sheng, Chin. J. Chem. Phys. **30**, 379 (2017).
[16] S. S. Wang, R. H. Kong, X. B. Shan, Y. W. Zhang, L. S. Sheng, Z. Y. Wang, L. Q. Hao, and S. H. Zhou, J. Synchrotron. Radiat. **13**, 415 (2006).
[17] S. Y. Chiang, M. Bahou, K. Sankaran, Y. P. Lee, H. F. Lu, and M. D. Su, J. Chem. Phys. **118**, 62 (2003).
[18] K. R. Wilson, L. Belau, C. Nicolas, M. Jimenez-Cruz, S. R. Leone, and M. Ahmed, Int. J. Mass spectrom. **249**, 155 (2006).
[19] K. Raghavachari, G. W. Trucks, J. A. Pople, and M. Head-Gordon, Chem. Phys. Lett. **589**, 37 (2013).
[20] T. H. Dunning, J. Chem. Phys. **90**, 1007 (1989).
[21] R. L. J. Grant and D. Smith, J. Phys. Chem. **100**, 18718 (1996).
[22] C. E. Smith, T. D. Crawford, and D. Cremer, J. Chem. Phys. **122**, 174309 (2005).
[23] B. J. Chen, P. Y. Tsai, T. K. Huang, Z. H. Xia, K. C. Lin, C. J. Chiou, B. J. Sun, and A. H. H. Chang, Phys. Chem. Chem. Phys. **17**, 7838 (2015).
[24] J. Chen, M. Q. Cao, B. Wei, M. M. Ding, X. B. Shan, F. Y. Liu, and L. S. Sheng, J. Mass Spectrom. **51**, 169 (2016).
[25] M. J. Frisch, G. W. Trucks, H. B. Schlegel, G. E. Scuseria, M. A. Robb, J. R. Cheeseman, G. Scalmani, V. Barone, B. Mennucci, G. A. Petersson, H. Nakatsuji, M. Caricato, X. Li, H. P. Hratchian, A. F. Izmaylov, J. Bloino, G. Zheng, J. L. Sonnenberg, H. Hada, M. Ehara, K. Toyota, R. Fukuda, J. Hasegawa, M. Ishida, T. Nakajima, Y. Honda, O. Kitao, H. Nakai, T. Vreven, J. A. Montgomery Jr., J. E. Peralta, F. Ogliaro, M. Bearpark, J. J. Heyd, E. Brothers, K. N. Kudin, V. N. Staroverov, R. Kobayashi, J. Normand, K. Raghavachari, A. Rendell, J. C. Burant, S. S. Iyengar, J. Tomasi, M. Cossi, N. Rega, J. M. Millam, M. Klene, J. E. Knox, J. B. Cross, V. Bakken, C. Adamo, J. Jaramillo, R. Gomperts, R. E. Stratmann, O. Yazyev, A. J. Austin, R. Cammi, C. Pomelli, J. W. Ochterski, R. M. Martain, K. Morokuma, V. G. Zakrzewski, G. A. Voth, P. Salvador, J. J. Dannenberg, S. Dapprich, A. D. Daniels, O. Farkas, J. B. Foresman, J. V. Ortiz, J. Cioslowski, and D. J. Fox, *Gaussian 09, Revision A.1*, Wallingford, CT: Gaussian, Inc., (2009).
[26] http://webbook.nist.gov/(Last accessed 2018).

DOI:10.1063/1674-0068/cjcp1805089